Exploring the Effect of Framework Flexibility on Water Adsorption in the Metal-Organic Framework NbOFFIVE-1-Ni Using Molecular Modelling

Hilal Daglar[a,b], Seda Keskin[a,*], Randall Q. Snurr[b,*]

[a]Department of Chemical and Biological Engineering, Koç University, Rumelifeneri Yolu, Sariyer, 34450, Istanbul, Turkey

[b]Department of Chemical and Biological Engineering, Northwestern University, 2145 Sheridan Road, Evanston, Illinois 60208, United States

Submitted to *The Journal of Physical Chemistry C*

Abstract

Many metal-organic frameworks (MOFs) are known to show complex structural flexibility such as breathing, swelling, and linker rotations, and understanding the impact of these structural changes on their guest adsorption properties is important in developing MOFs for practical applications. In this study, we used a multi-scale computational approach to provide a molecular-level understanding of how flexibility affects water adsorption in the MOF, NbOFFIVE-1-Ni. This material has narrow pores and good hydrothermal stability, which make it attractive for CO_2 capture. We utilized density functional theory (DFT) calculations and grand canonical Monte Carlo (GCMC) simulations to study the impact of NbOFFIVE-1-Ni structural flexibility on its water adsorption at different humidity conditions. Studying the water adsorption in different configurations of NbOFFIVE-1-Ni demonstrated that DFT optimization in the presence of adsorbed water molecules and rotating the linkers are useful strategies to mimic its structural flexibility. Our results illustrate the significance of taking structural flexibility into account when designing MOFs for water adsorption and other relevant applications.

Keywords: metal-organic framework, flexibility, linker rotation, water adsorption, molecular simulation

*Corresponding authors: e-mail: skeskin@ku.edu.tr and snurr@northwestern.edu

1. Introduction

Metal-organic frameworks (MOFs) are porous crystalline materials formed by self-assembly of inorganic and organic building blocks.[1] Thanks to their high porosities,[2] large surface areas,[3] and tunable chemical functionalities,[4] they have emerged as promising materials for various applications from gas storage and separation[5] to catalysis.[6, 7] Given the large number of existing MOFs, molecular simulations can play a pivotal role in predicting MOF performance for a target application prior to experimental efforts. Simulations can also provide molecular-level insights that may lead to the rational design of materials having desired properties. In molecular simulations, MOFs have generally been modeled as rigid frameworks to save computational time and reduce the complexity of the simulations. On the other hand, many MOFs have been reported to exhibit structural flexibility, such as breathing, swelling, and linker rotations, as a response to external stimuli such as pressure, temperature, or the presence of guest molecules.[8, 9] The flexibility of MOFs is a complex and critical aspect of their functionality that can change their guest adsorption properties. For example, the adsorbed guest molecules inside the pores of a flexible MOF can trigger a structural transition, resulting in changes in pore size, which, in turn, affects the amount of gas adsorbed.[10, 11]

Molecular simulations play a critical role in understanding flexibility and phase transitions in MOF materials and in improving our understanding of the microscopic mechanisms that govern gas adsorption in flexible MOFs. Several computational studies have investigated the effect of MOF flexibility on the guest adsorption properties for specific applications, such as CO_2 capture[12-16] and CH_4 storage.[17-20] Water adsorption has a critical role in many important applications such as direct air capture, CO_2 capture from wet flue gas, and water harvesting, but molecular simulation studies on water adsorption are challenging for several reasons:[21] (i) Polar water molecules can form hydrogen bonds with the MOF atoms, which complicates the energy calculations in molecular simulations, (ii) the formation of adsorbed water clusters can trap the water-MOF system in a local free energy minimum, making it difficult to reach equilibrium,[22] (iii) selection of a water model that accurately mimics all the key properties of bulk water is not straightforward.[23, 24] Thus, molecular simulation of a flexible MOF for water adsorption presents a series of challenges that arise from the intrinsic properties of MOFs and the complexities of modeling of water as a guest molecule.

A limited number of computational efforts exist that focus on the impact of the structural flexibility of MOFs on their water adsorption properties. Maurin et al.[25] performed grand canonical Monte Carlo (GCMC) and molecular dynamics (MD) simulations to examine the effect of the breathing behavior of a MOF, MIL-53, on its water adsorption properties. Their results showed that while the large-pore form of MIL-53 is mildly hydrophobic, with the water molecules forming clusters, the narrow-pore version is hydrophilic, with strong interactions between the water molecules and the pore walls. Devautour-Vinot et al.[26] integrated complex impedance spectroscopy measurements and density functional theory (DFT) calculations to study the preferential arrangements of water molecules in the pores of flexible MIL-53 (Cr) and MIL-53(Fe). Coudert et al.[27] performed DFT-based MD simulations to shed light on the structural response of MIL-53(Ga) to adsorbed water molecules, and their results showed that water adsorption in this MOF involves an intermediate structure between the narrow-pore and large-pore versions of the material. By performing GCMC simulations, Grenev et al.[28] studied the framework flexibility of CAU-10-H to investigate the mechanism of water adsorption, and their simulation results showed that the linker "flapping" motion of the framework affects the framework hydrophilicity and, thereby, the adsorbed water amount. Previous studies also revealed that the effect of flexibility on gas adsorption is more pronounced for narrow-pore MOFs compared to MOFs having large pores.[29, 30]

In this work, we examined the impact of the structural flexibility of the MOF NbOFFIVE-1-Ni on its water adsorption properties. This is an interesting ultra-microporous material, which is reported to be hydrolytically stable and a promising candidate for direct air capture of CO_2 with the highest CO_2 uptake at low concentrations (400 ppm) and 298 K.[31] In addition, structural changes were studied in NbOFFIVE-1-Ni during propane/propylene separation, and the diffusion of gas molecules in this structure was reported to depend on the structural flexibility of the MOF.[32] Motivated by these reports, we examined the framework flexibility of NbOFFIVE-1-Ni and its synergistic effects on the water adsorption behavior of this MOF. We utilized a multi-scale computational approach, combining quantum chemical calculations with classical molecular simulations to understand the structural transitions of NbOFFIVE-1-Ni during water adsorption. To avoid computationally intensive ab initio MD simulations – and due to the lack of a validated force field to directly model the flexibility of this MOF – we generated different configurations of NbOFFIVE-1-Ni to mimic its structural flexibility and used these structures as inputs to GCMC

simulations of water adsorption. In our first approach, DFT calculations were performed to determine the optimized derivatives of NbOFFIVE-1-Ni representing the structure at different humidity levels. In our second approach, the linkers of NbOFFIVE-1-Ni were rotated by different degrees to mimic the framework flexibility reported by Dyer and coworkers.[32] By performing GCMC simulations of water adsorption in these different structures, we obtained their simulated water adsorption isotherms and compared them with the reported experimental water adsorption isotherm.[31] Our results shed light on the structural flexibility of NbOFFIVE-1-Ni and its water adsorption performance.

2. Computational Methods

Structure modeling: We obtained the structure of NbOFFIVE-1-Ni (as-made composition: $[Ni(NbOF_5)(C_4H_4N_2)_2 \cdot 2H_2O]$), also known as KAUST-7, from the Cambridge Structural Database (deposition number 1505385). **Figure 1** shows the image of a 3×3× 2 supercell of NbOFFIVE-1-Ni. In the experimental structure,[31] the $(NbOF_5)^{2-}$ anion site was reported with a mixed occupancy F:O of 0.5:0.5. We manually fixed the number of F and O atoms based on the chemical formula of NbOFFIVE-1-Ni and created three different versions of the framework by changing the arrangement of O and F atoms of $(NbOF_5)^{2-}$ polar units as shown in **Figure S1.** A series of DFT calculations were performed for different orientations of $(NbOF_5)^{2-}$ anions defined by the positions of F and O atoms. We utilized the periodic DFT calculations to identify the structure with the lowest energy. We used the VASP-recommended v.5.4.4[33, 34] projector-augmented waves (PAW) potentials for all elements.[35] The cutoff energy was set to 600 eV for the plane-wave expansion of the wave function. The PBE density functional with D3(BJ) empirical dispersion correction was applied to account for the long-range van der Waals interactions.[36-38] Energy convergence was 10^{-6} eV for the self-consistent field (SCF) cycles, and the force convergence was set to 0.01 eV/Å for geometry optimization. We used a Monkorst-Pack Gamma (Γ)-centered 2×2×2 k-point mesh. During geometry optimizations, we considered both keeping the lattice parameters constant (ISIF=2) and fully optimizing the atomic positions and lattice parameters (ISIF=3). We also tested the DFT+U method[39] with the Hubbard correction term[32] of U=6.45 eV to correct for the self-interaction error introduced by highly localized d orbitals of Ni atoms. The additional U term allows for more accurate modeling of structures with d electrons.[40]

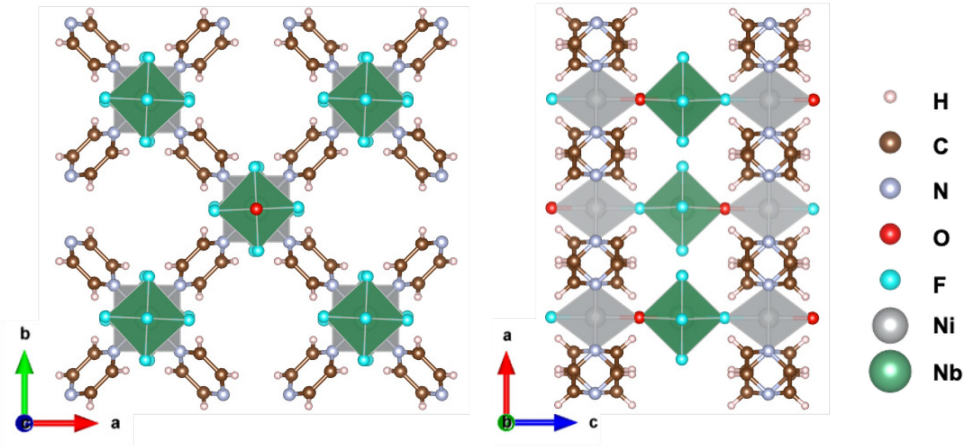

Figure 1. NbOFFIVE-1-Ni shown from two directions.

Adsorption calculations: We performed GCMC simulations using the RASPA 2.0.37 software[41] to compute H_2O and CO_2 uptakes in NbOFFIVE-1-Ni. The Lennard-Jones (LJ) 12-6 potential was used to describe the dispersion and repulsion interactions between non-bonded atoms using a cut-off distance of 12.8 Å without tail corrections. LJ parameters for the framework atoms were taken from the Universal Force Field (UFF),[42] and the Lorentz-Berthelot mixing rules were used to obtain LJ parameters between different pseudo-atoms. The long-range Coulombic interactions were calculated by the Ewald summation with a precision of 10^{-6}.[43] To assign partial charges to the framework atoms, we used the Density Derived Electrostatic and Chemical (DDEC6) method for each structure.[44, 45] Periodic boundary conditions were applied in all three dimensions by using a 3×3×2 supercell, and the structures were assumed to be rigid during the simulations to save computational time.

The CO_2 molecule was represented as a three-site molecule in which two sites were positioned at the O atoms with charges of -0.35, and the third site was at the C atom with a charge of 0.70.[46] For the H_2O molecule, the rigid 4-site TIP4P model (saturated vapor pressure, P_{sat} = 4714 Pa at 298 K without tail corrections) in which the center of mass (L-H_2O) site with a partial point charge of -1.04 and H-H_2O with charges of 0.52 was used.[42] This model provides a better estimation for the saturated vapor pressure around 300 K compared to other water models.[47] All LJ parameters used for NbOFFIVE-1-Ni and guest molecules (CO_2 and H_2O) are given in **Table S1**. For each point on the isotherm, we used 200,000 cycles for equilibration and 500,000 cycles for production. A cycle is a max (20, n) move attempts, with n being the number of adsorbed molecules.[41] In the molecular simulations, the fugacity coefficients were assumed to be one.

Translation, rotation, reinsertion, and configurational bias swap (insertion/deletion) moves were utilized in the simulations.

3. Results and Discussions

3.1. Validation of the structure modeling

Figure 2 shows the structure of NbOFFIVE-1-Ni with three different possible orderings for the O and F atoms in the $(NbOF_5)^{2-}$ anions. We will refer to the structures as the nonpolar (individual $(NbOF_5)^{2-}$ dipoles cancel each other), polar-I and polar-II (individual $(NbOF_5)^{2-}$ dipoles are additive) structures. **Table S2** shows the relative DFT energies of the three structures. We used the DFT energy of the nonpolar structure as a reference value, and the results showed that the polar structures have lower DFT energies than the nonpolar one. Since the polar-II structure, with strictly alternating positions of axial O and F atoms and identical orientations of equivalent pyrazine molecules in adjacent Ni-pyrazine layers, has the lowest relative DFT energy, we used it in the subsequent calculations. Note that the DFT energy differences in **Table S2** for the two polar structures are at the edge of DFT accuracy;[48, 49] thus, both polar structures (-I or -II) could be used in the molecular simulations. Considering the structure used in the previous computational study[32] of NbOFFIVE-1-Ni, we chose the optimized version of the polar-II structure for subsequent calculations. Throughout the manuscript, the default DFT setup parameters are PBE+D3(BJ) with the lattice parameters kept constant (ISIF=2).

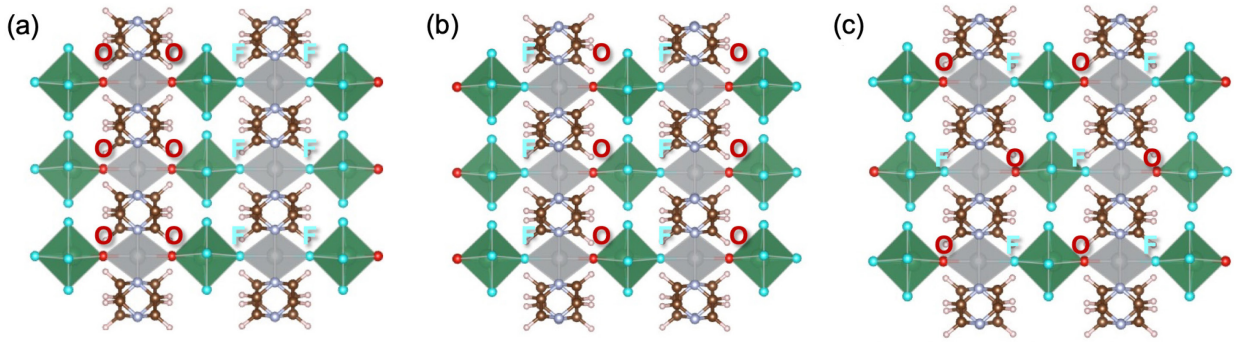

Figure 2. NbOFFIVE-1-Ni structures with different orientations of $(NbOF_5)^{2-}$ anions (shown as green polyhedra) with (a) nonpolar, (b) polar-I, (c) polar-II alignments. The order of O (red) and F (turquoise) atoms are highlighted with red circles. The atom colors are defined in Figure 1.

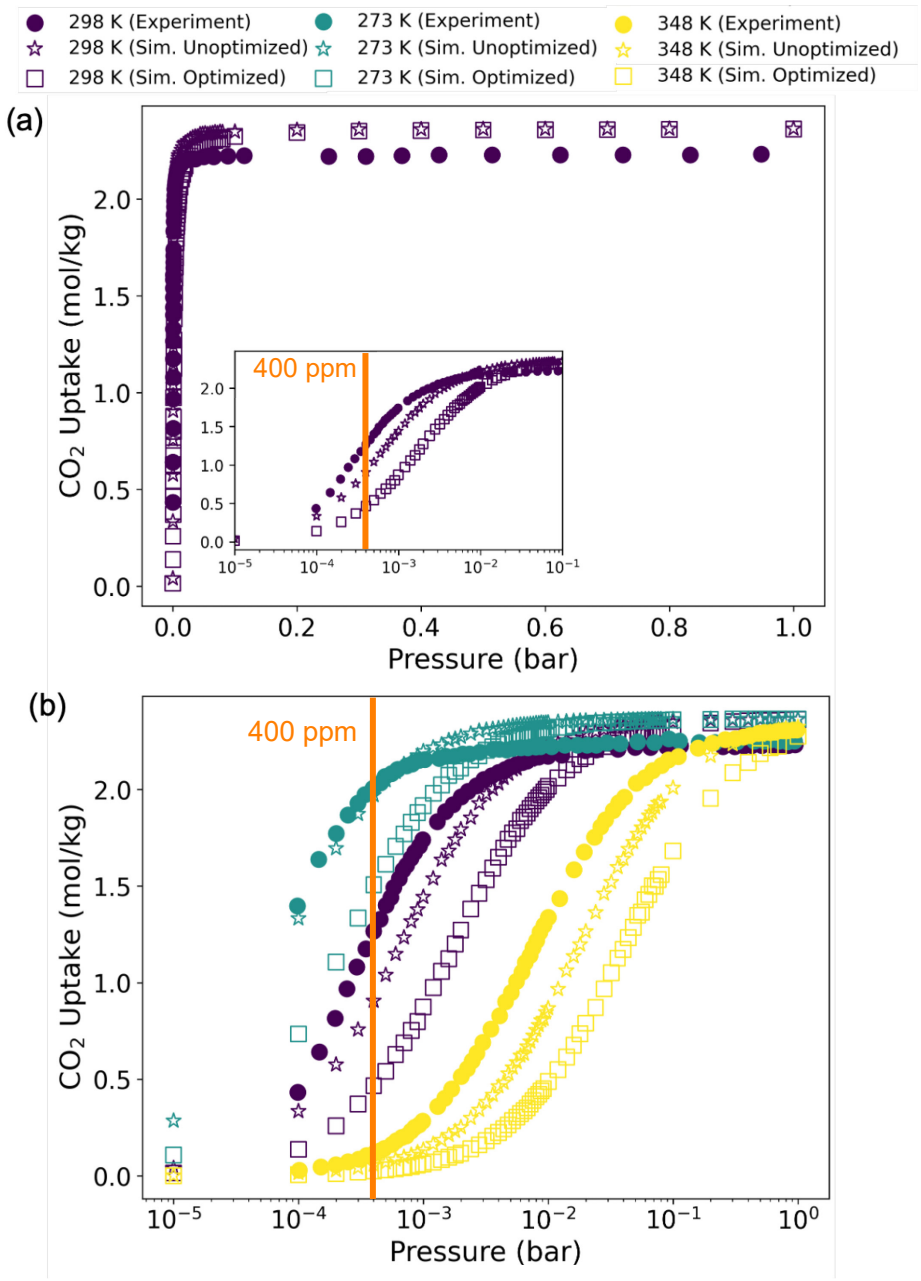

Figure 3. CO_2 adsorption isotherms for NbOFFIVE-1-Ni (a) at 298 K and (b) at 273, 298, and 348 K. Filled symbols represent experimentally reported[31] data. The orange line shows the concentration of CO_2 (400 ppm) in direct air capture.

We first validated our molecular simulations and the selected polar structure (polar-II) by computing the CO_2 adsorption isotherms of the DFT-optimized and unoptimized NbOFFIVE-1-Ni structures and comparing the isotherms with the experimentally reported[31] CO_2 adsorption isotherms. Note that a semi-logarithmic scale was used for **Figure 3** to make differences at the low loading data more easily seen,[31] specifically at 400 ppm CO_2 concentration, which is relevant for

direct air capture application. **Figure 3(a)** shows that the simulated CO_2 adsorption isotherms at 298 K show a similar trend as the experimental isotherm, although the simulated isotherms underestimate the experiment at low pressure and slightly overestimate the experimental values at high pressure. At low pressure, the optimized structure shows consistently lower CO_2 uptakes compared to the unoptimized structure. At pressures higher than 0.01 bar, the simulated CO_2 uptakes for unoptimized and optimized structures are quite similar. **Figure 3(b)** compares the simulated CO_2 isotherms with experiment at various temperatures. At 273 K, 298 K, and 348 K, the coefficient of determination (R^2) between the simulated CO_2 adsorption isotherms (in the range of 0.00001-1 bar) of the optimized and unoptimized structures are 0.66, 0.76, and 0.82, respectively. On the other hand, the root mean square error (RMSE) between the unoptimized and optimized isotherms were calculated as 0.19, 0.30, and 0.31 mol/kg, respectively. To compare experimental CO_2 adsorption isotherms with simulated ones, we calculated the area under the curve (AUC), which is a metric for the whole isotherm shape, RMSE and the mean absolute error (MAE) for the CO_2 adsorption isotherms in **Figure 3(b)** at different temperatures, as shown in **Table S3.** AUC values for the simulated CO_2 adsorption isotherms obtained from the unoptimized and optimized structures are very similar to one another and are higher than the AUC for the experimental isotherm at 273 K. They align better with the experimental data as the temperature increases. On the other hand, RMSE and MAE values between experimental isotherms and simulated ones (in the range of 0.00001-1 bar) increase when temperature increases. The experimentally reported[31] heat of adsorption values for CO_2 (50.2-54.8 kJ/mol) are also similar to the values we computed (54.2-54.7 kJ/mol) using GCMC, suggesting that molecular simulations accurately predict the experimental data.

Motivated by the reasonable agreement between simulated and experimental data for CO_2, GCMC simulations for H_2O adsorption were performed at 298 K between 0 and 100% relative humidity (RH), where RH% was defined as $(P / P_{sat})\times 100$. Note that we performed GCMC simulations until the loading values did not change with additional simulation cycles. Additionally, we obtained error bars for the simulation results by splitting the simulation into five blocks and calculating the standard deviation of the block averages, which is computed as the 95% confidence interval. **Figures S2-S3** show that the water adsorption simulation results we computed in this study have converged and resulted in median errors below 6%.

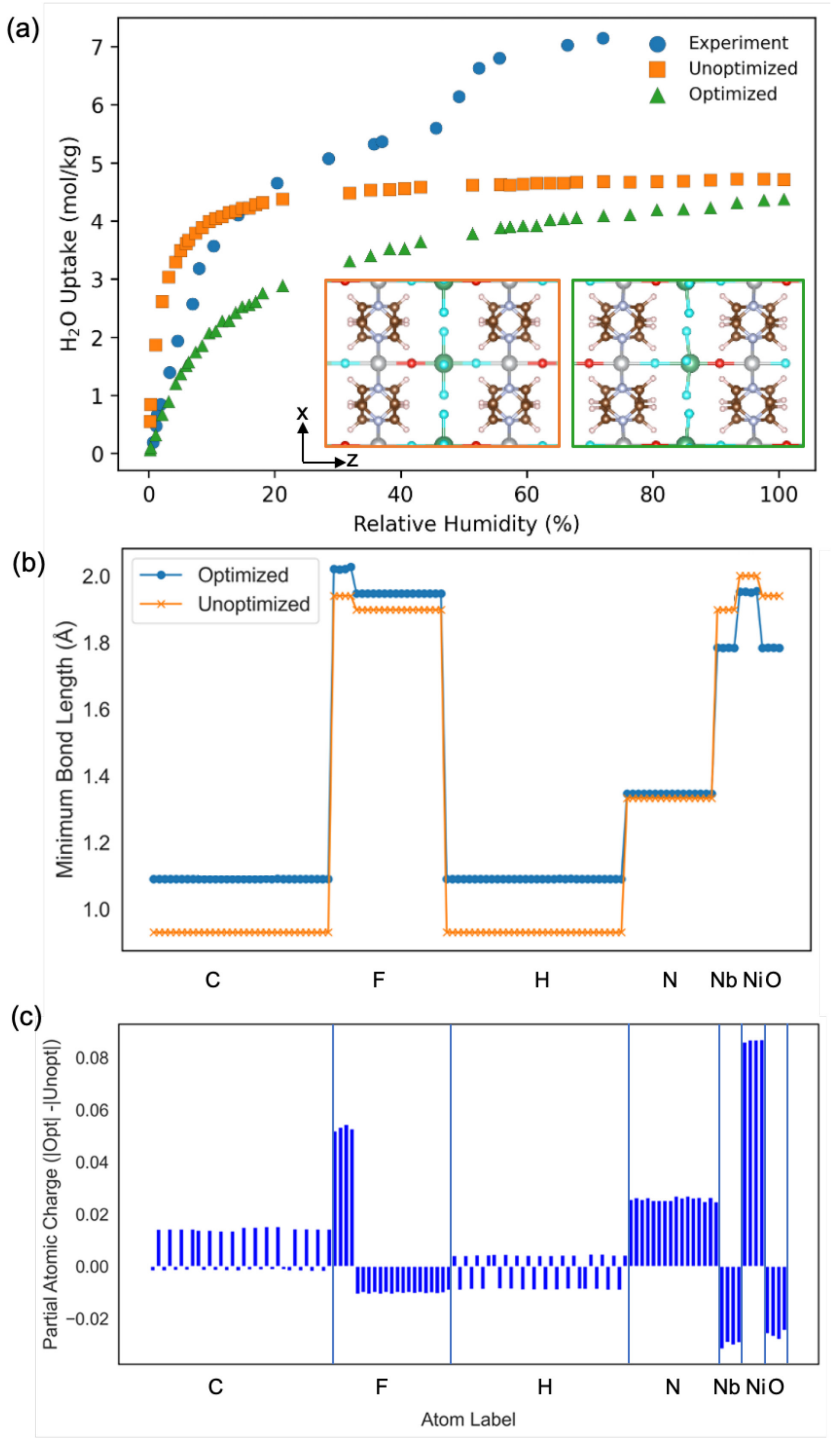

Figure 4. Effect of DFT optimization of NbOFFIVE-1-Ni: (a) Comparison of simulated water adsorption isotherms for DFT-optimized and unoptimized structures with the experimental data.[31] The insets show the snapshots of unoptimized and optimized structures in orange and green boxes, respectively. (b) Minimum bond lengths for C, F, H, N, Nb, Ni, and O atoms in unoptimized and optimized structures. (c) Differences in partial atomic charges of NbOFFIVE-1-Ni, obtained by subtracting the absolute charge values of each atom in the optimized structure from those of the corresponding atom in the unoptimized structure.

Figure 4(a) shows the comparison of water adsorption isotherms obtained from simulations using the optimized and unoptimized structures with the experimentally reported isotherm.[31] Below about 15% RH, the simulated results for the unoptimized structure overestimate the experimental isotherm, and the simulated results for the optimized structure underestimate the experimental isotherm. At very low humidity (0-5% RH), the simulated results for the optimized structure are quite close to the experimental data. Radial distribution function (RDF) analysis in **Figure S4** shows strong interactions between the H atoms of water and the F atoms of the MOF's anionic pillars. Similar to the experimental isotherm, the simulated water adsorption of the unoptimized structure showed a rapid increase (up to 4.3 mol/kg) in the low RH region. Above 20% RH, the simulated isotherm of the unoptimized structure shows a plateau, while the simulated isotherm of the optimized structure exhibits a more gradual increase. However, the simulated water uptake values of both structures underestimate the experimental water uptake above 20% RH and do not exhibit the second step observed in the experimental isotherm around 55% RH.

To understand how DFT optimization affects the structure of NbOFFIVE-1-Ni and hence its water uptake, we compared the bond lengths, atomic positions, and partial atomic charges of the framework before and after optimization. When the structure is optimized, atomic positions slightly change as shown in **Figure S5**, and the minimum bond lengths for all atoms except N atoms change as shown in **Figure 4(b)**. The resulting partial charges on the F atoms of the optimized structure are generally lower in magnitude compared to the charges of the unoptimized structure as shown in **Figure 4(c)**. We also performed GCMC simulations for the DFT-optimized structure using the DDEC charge values of the unoptimized structure. The results showed a slight increase in the simulated water adsorption isotherms as shown in **Figure S6**. Thus, we inferred that changes in both the electrostatic interactions and the structure affect the water isotherm, but the change in structure plays a more important role in making the simulated isotherm lower in the optimized structure compared to the unoptimized structure.

3.2 Effect of DFT optimization with adsorbed water

We adopted two strategies to investigate how the presence of water affects the structural and electrostatic environment inside NbOFFIVE-1-Ni. In the first approach, we inserted different numbers of water molecules in the pores of the framework and performed a DFT optimization of the MOF plus water molecules using the same DFT methods as described above. To provide a good initial configuration for each DFT calculation, we first performed an energy minimization

with the classical force field (and rigid MOF) and then ran a short MC simulation in the NVT ensemble[41] to relax the configurations of the guest molecules. After DFT optimization, we removed the water molecules from the optimized structure and ran GCMC simulations holding the MOF rigid at the configuration from the DFT calculation.

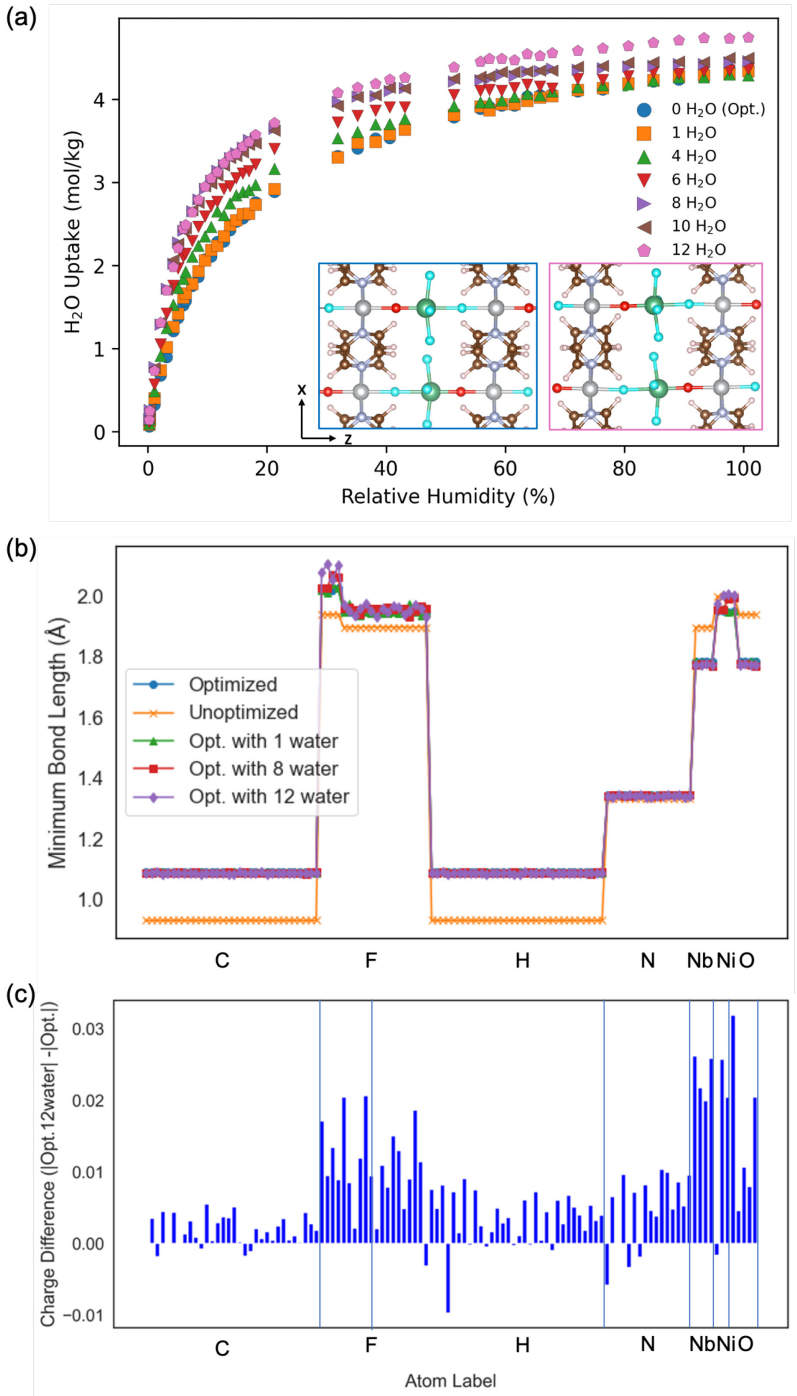

Figure 5. Effect of DFT optimization of NbOFFIVE-1-Ni in the presence of water: (a) Simulated water adsorption isotherms of DFT-optimized structures with 1, 4, 6, 8, 10, and 12 water molecules

per unit cell. The insets show snapshots of the DFT-optimized structures with 0 and 12 water molecules in blue and pink boxes, respectively. (b) Minimum bond lengths for C, F, H, N, Nb, Ni, and O atoms in optimized structures with 0, 1, 8, or 12 water molecules inserted and the unoptimized structure. (c) The differences in partial atomic charges of NbOFFIVE-1-Ni atoms, obtained by subtracting the absolute charge value of each atom in the optimized structure with 12 water molecules from that of the corresponding atom in the unoptimized structure.

Figure 5(a) shows the water adsorption isotherms using the structures that were DFT-optimized with 1, 4, 6, 8, 10, or 12 adsorbed water molecules per unit cell (which were then removed before performing the GCMC simulations as described above), corresponding to loadings of 0.59, 2.4, 3.5, 4.7, 5.9, and 7.1 mol H_2O/kg MOF, respectively. In all cases, the isotherms display Type I isotherm shapes. As the number of water molecules present during DFT optimization increases, the GCMC loading increases in the range of 0-40%, and there is some crossing of the isotherms above 40% RH. Similarly, Shukla et al.[50] investigated the effect of structural changes of UiO-66 on the adsorption of acetone and showed that when the number of inserted acetone molecules in UiO-66 increases, the acetone adsorption of the structures increases. DFT optimization at different water loadings slightly affects the atomic positions within the structure as shown in **Figures S7-S9**. For instance, the inset images in **Figure 5(a)** demonstrate how the atomic positions shift in the x and z-directions after DFT optimization in the presence of 12 water molecules.

Figure 5(b) shows how the minimum bond lengths between the framework atoms are altered in the presence of water. In most cases, there is very little effect of the water molecules, but there are some differences for the F atoms, which are present in the $(NbOF_5)^{2-}$ anions. **Figure 5(c)** presents the difference between the partial charges of the original structure (no water molecules) and the corresponding charges of the optimized structure using 12 water molecules. Partial atomic charge values of the optimized structure used as the reference data in **Figure 5(c)** are provided in **Table S4**. The differences in atomic charge range between -0.01 and +0.03, with values generally higher in magnitude in the structure optimized with 12 water molecules. This illustrates that the changes in the atomic positions of $(NbOF_5)^{2-}$ anions affect the distribution of partial atomic charges. Specifically, the increase in the magnitude of F charge values may contribute to enhanced water adsorption. The changes in the partial atomic charges of the DFT-optimized structures with 1, 4, 6, 8 and 10 water molecules are depicted in **Figure S10**. To test if the changes in the simulated water isotherms were primarily due to changes in the structure or changes in the framework partial

charges, we repeated the GCMC simulations for the DFT-optimized structures at various water loadings using the partial atomic charges assigned to the original structure without adsorbed water molecules. **Figure S11** shows the results, which are generally similar to those in **Figure 5(a)**, indicating that the effects in **Figure 5(a)** are mainly due to structural changes resulting from the DFT optimization, and to a lesser extent, small differences in the framework partial charges.

We further investigated the effects of setup parameters on the final DFT energy values, specifically examining the impact of maintaining constant lattice parameters and incorporating the Hubbard correction factor for the highly localized d orbitals of Ni atoms. **Table S5** shows the relative DFT energies calculated using different numbers of adsorbed water molecules. For each loading of water molecules, the energies calculated by keeping the lattice parameters constant (ISIF=2) and optimizing atomic positions and lattice parameters (ISIF=3) are very close to each other, both with and without the +U correction. This similarity indicates that the different setup parameters for DFT optimization provide comparable results, thereby enhancing the robustness of our simulation outcomes. Therefore, we presented the water adsorption results from DFT optimization (PBE+D3(BJ)) with the lattice parameters kept constant. **Table S6,** which presents lattice constants and lattice angles for the unoptimized and ISIF=3 structures (both DFT and DFT+U), shows that the changes in lattice parameters after DFT optimization are negligible.

3.3. Effect of linker rotation

In the second approach to mimic structural flexibility in the presence of adsorbed water, we considered the effect of linker rotation, motivated by previous work[32] suggesting that the pyrazine linkers of NbOFFIVE-1-Ni rotate during the diffusion of guest molecules. Using the rotation tool in the Materials Studio software (2020),[51] we rotated the pyrazine linkers around the axis that is equally inclined to the x and y axes, to various degrees as shown in **Figure 6**. All pyrazine linkers were rotated simultaneously by the same angle, and we obtained eight linker-rotated derivatives of the structure, using increments of 7° for each rotation. All linker rotated derivatives of NbOFFIVE-1-Ni are shown in **Figure S12**.

We then performed GCMC simulations in these (rigid) structures to understand the effect of linker rotation on the simulated water adsorption isotherms. **Figure 6** shows images of the original structure and two linker-rotated derivatives of NbOFFIVE-1-Ni, representing a “planar” structure with a 28.3° rotation and a rotation of 56.6°, which brings the linker back to its original angle although with some small changes in the structure. Moving from the original structure (0° rotation)

to the planar structure (28.3° rotation), the pore limiting diameter increases from 3.60 Å to 4.11 Å (**Table S7**). **Table S7** also shows that while the pore sizes of the linker-rotated derivatives vary in the range of 3.6-4.1 Å, the pore volumes and void fractions do not show much variation, with values of 0.23-0.24 cm^3/g and 0.43-0.44, respectively.

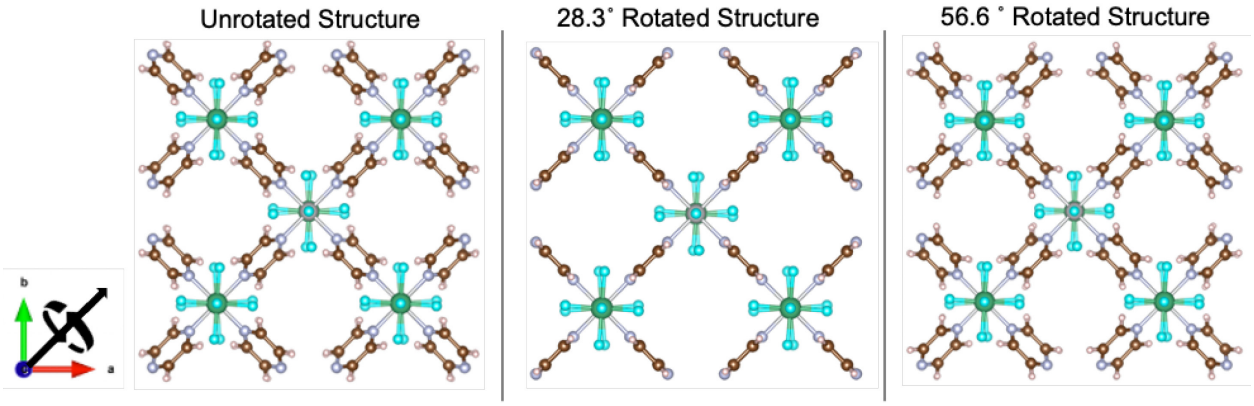

Figure 6. Structures of NbOFFIVE-1-Ni with different degrees of linker rotation. The black arrow shows the rotation axis.

Figure 7(a) presents the water adsorption isotherms of eight linker-rotated derivatives of NbOFFIVE-1-Ni at 298 K. Below 40% RH, as the linker rotation increases from 0° to 28.3°, the water uptake decreases. This can be explained by the increase in pore size, which leads to lower adsorption at low pressure. At high RH (>50%), higher degree of linker rotation up to 28.3° (and larger pore sizes) leads to higher water uptake values compared to the unrotated structure. Note that due to symmetry, angles of 0° and 56.6°, 7° and 49°, 14° and 42°, 21° and 35° are similar to each other, although the optimized structures are not identical, leading to small differences in the water isotherms. At low RH, a similar but weaker trend between the water adsorption isotherms of structurally similar derivatives is observed. For instance, water uptakes of the linker-rotated structure with 56.6° below 40% RH are generally higher than those of the unrotated structure because of the difference in charge distribution.

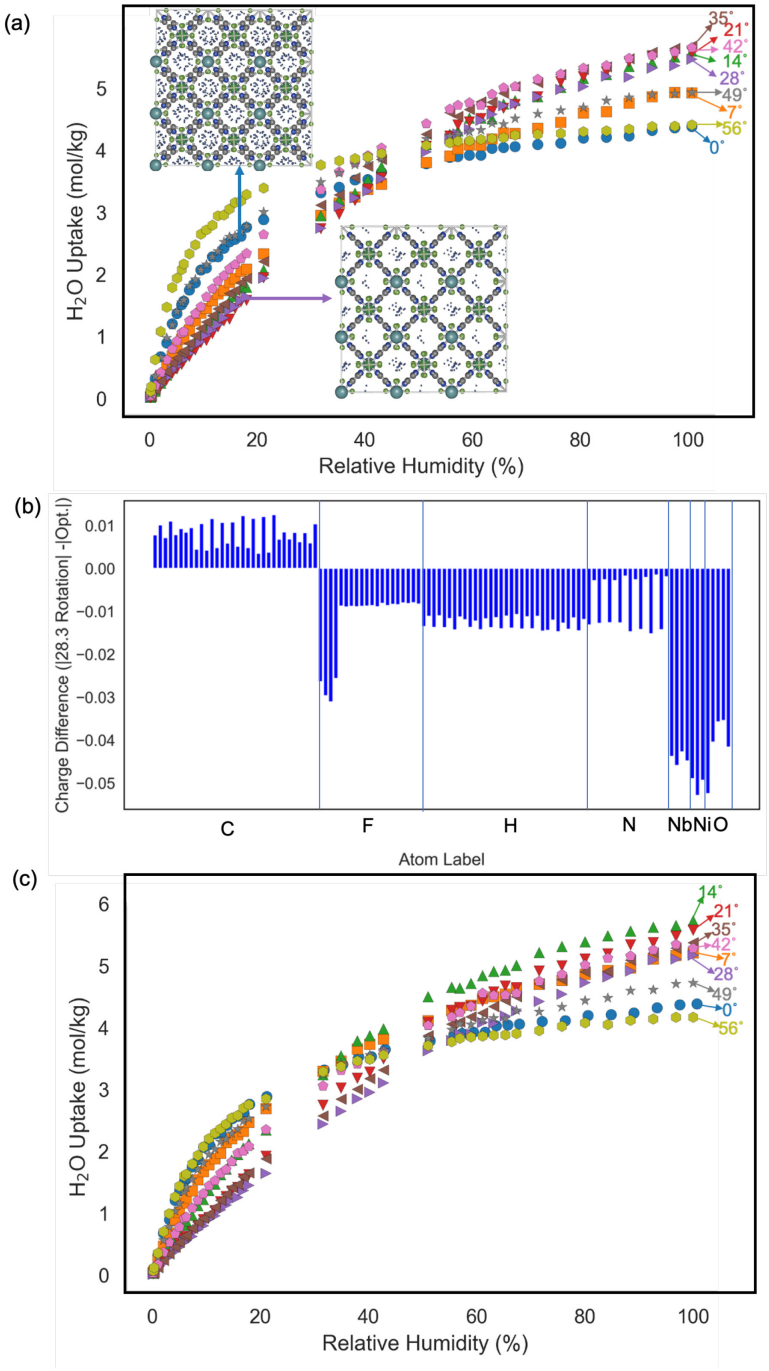

Figure 7. Effect of linker rotation of NbOFFIVE-1-Ni: (a) Comparison of simulated water adsorption isotherms at 298 K for linker-rotated derivatives of NbOFFIVE-1-Ni. The inset snapshots show the distribution of water molecules for the unrotated and 28.3°-rotated derivatives of NbOFFIVE-1-Ni at 20% RH. (b) The differences in partial atomic charges of NbOFFIVE-1-Ni, obtained by subtracting the absolute charge values of each atom in the 28.3°-rotated structure from those of the corresponding atoms in the unrotated structure. (c) Comparison of simulated water adsorption isotherms for the linker-rotated derivatives of NbOFFIVE-1-Ni obtained from the GCMC simulations where the partial atomic charge values of the framework atoms of the unrotated (0°) structure were used.

Since we calculated DDEC charges for each derivative structure, we calculated the difference in magnitude of the partial charges between the framework with linkers rotated by 28.3° and the original (unrotated) structure as shown in **Figure 7(b)**. Assigned charge values for the structure with 28.3° linker rotation were generally lower in magnitude than those of the unrotated structure, resulting in decreased water uptake at low RH. We also compared the charges in the original structure and in the structure with the linkers rotated by 56.6°, since these structures should be similar due to symmetry. As shown in **Figure S13**, the partial charge values of the F atoms in the structure with the linkers rotated by 56.6° are slightly higher than those in the unrotated structure, suggesting that variations in the electrostatic interactions could be responsible for the differences in the simulated water adsorption observed at low RH.

To deconvolute the effect of changes in the structure and changes in the partial charge values upon linker rotation, we performed the GCMC simulations using the framework charges of the unrotated structure for all linker-rotated derivatives. The results are shown in **Figure 7(c)**. Similar structures such as 0° and 56° and 21° and 35° exhibit similar water uptakes as expected. Also, even though the charges are the same for all structures, significant differences exist in the isotherms for different degrees of linker rotation, suggesting that the different pore geometries are, indeed, responsible for the differences observed in **Figure 7(a)**. We can draw three conclusions regarding the linker rotation of NbOFFIVE-1-Ni: (i) All of the simulated isotherms of the NbOFFIVE-1-Ni derivatives are Type I although water uptakes dramatically change based on the angle of linker rotation. (ii) Linker rotation changes the pore geometry of NbOFFIVE-1-Ni, which causes a decrease in water uptake at low RH but results in an increase in water uptake at high RH. (iii) Partial charges have a slight effect on the water uptake values of linker-rotated derivatives of NbOFFIVE-1-Ni but not on the shape of the isotherm for similar structures. Note that we rotated all linkers in the structure at the same angle to investigate the relationship between the rotation angle of linkers (with 7° increments) and the water adsorption isotherm of NbOFFIVE-1-Ni. However, in the real system, effects such as temperature and the presence of guest molecules would likely cause each linker to rotate to a different angle. Therefore, having all linkers rotate together is a limiting case in fully understanding the rotational linker dynamics of the framework.

3.4. Final assessment of water adsorption isotherms

Figure 8(a) compares simulated water adsorption isotherms of representative NbOFFIVE-1-Ni derivatives with the experimentally reported isotherm. We note that our goal in this study was not to tune the model to reproduce the experimentally reported water adsorption isotherm but to understand how changes in the framework structure affect the simulated water adsorption isotherm. All simulated isotherms are Type I, and none of the simulated isotherms show the step observed in the experimental isotherm. The highest water uptake (5.8 mol/kg for the structure with the linkers rotated by 28.3°) obtained from the simulations is significantly below the experimentally reported saturation loading (~6.8 mol/kg). One possible reason for this is that the $(NbOF_5)^{2-}$ anions in the linker-rotated derivatives are kept fixed, which may prevent us from observing potential pore expansion and the formation of new adsorption sites for guest molecules.[32]

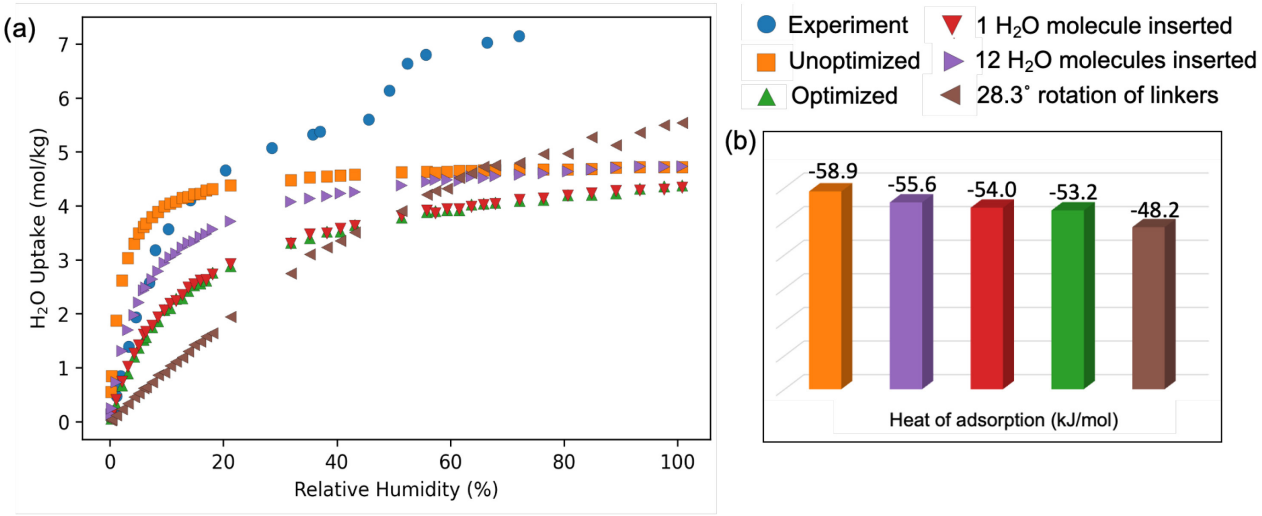

Figure 8. (a) Comparison of experimentally reported water adsorption isotherm[31] with the simulated isotherms of representative structures obtained from different computational methods. (b) The heats of adsorption (kJ/mol) at 2% RH of representative derivatives of NbOFFIVE-1-Ni.

At low RH, simulations using the experimental structure (orange) overestimate the experimental isotherm, and simulations using the DFT-optimized structure (green) underestimate the experiments. The discrepancy between the DFT-optimized and unoptimized structures arises primarily due to differences in MOF-gas interactions affected by both electrostatic and structural changes as we discussed in section 3.1. The calculated heats of adsorption also indicate that the interaction with water at low concentrations is stronger in the unoptimized structure (-58.9 kJ/mol) compared to the interactions in the optimized structure (-55.6 kJ/mol). The fact that the

experimental water uptakes at low RH% are between these two simulated ones from optimized and unoptimized structures demonstrates how even small changes in the NbOFFIVE-1-Ni structure due to optimization can be important in reproducing the experimental water adsorption. Rotating the linkers lowers the simulated isotherm even more (brown). Inserting 12 water molecules, corresponding to ~7 mol/kg, during the DFT optimization results in a simulated isotherm (purple) in close agreement with the experiment up to approximately 3 mol/kg. The heats of adsorption for water in the Nb OFFIVE-1-Ni derivatives at very low (2%) RH are shown in **Figure 8(b)**, and the order is as follows: unoptimized structure > DFT-optimized structure with 12 molecules inserted > DFT-optimized structure with 1 molecule inserted > DFT-optimized structure without water molecules inserted > linker-rotated (28.3°) structure. Both H_2O uptake and heat of adsorption for H_2O follow the same order, suggesting that the entropic effects are similar in all structures.

The most prominent feature of the experimental isotherm is the sharp step around 50% RH. Given that no simulation in a rigid structure exhibited an isotherm with a step, we hypothesize that the step is due to a structural transition brought about by adsorption of water. One could imagine that the experimental isotherm results from following one curve in **Figure 8(a)** up the RH of the structure transition and then jumping to another curve.[52] Recent work has suggested structural transformations in the related MOF SIFSIX-3-Ni.[53] However, the nature of this structural transition in NbOFFIVE-1-Ni is unknown at this point, and none of the structures that we simulated match the saturation loading seen in the experimental isotherm. It is also interesting that none of the DFT optimizations conducted with varying numbers of water molecules resulted in a rotation of the pyrazine linkers of NbOFFIVE-1-Ni. In situ PXRD studies and ab initio MD simulations would be useful to test this hypothesis.

4. Conclusions

In this work, we utilized a multi-scale approach to investigate the effect of proposed structural flexibility of an ultra-microporous MOF, NbOFFIVE-1-Ni, on its water adsorption isotherm. To mimic possible changes in the MOF structure during water adsorption, we created 14 derivatives of NbOFFIVE-1-Ni by performing DFT optimization of the structure at different water loadings and by rotating the pyrazine linkers in the framework. The DFT calculations showed that the $(NbOF_5)^{2-}$ anions of the structure move slightly in the presence of water molecules. We then

performed GCMC simulations in these (rigid) structures to obtain the water isotherm for each derivative at 298 K. Our GCMC results show that optimization of the structure in the presence of guest molecules and the rotation of the pyrazine linker considerably affect the water adsorption behavior of NbOFFIVE-1-Ni. In the approach of optimizing the structure at different water loadings, water uptake increases with increasing number of water molecules inserted in the DFT optimization. Rotating the pyrazine linkers changes the pore size, and larger pores lead to decreased uptake at low RH and increased uptake at high RH. No simulations in a (single) rigid structure yielded a stepped isotherm, as seen in the experiment. However, our results do show that the water adsorption isotherms are sensitive to changes in the MOF structure. We hypothesize that the step in the experimental water isotherm is due to a structural transformation of the MOF around 50% RH, but the nature of the transformation is not known at this time. In situ PXRD studies and ab initio MD simulations would be useful to test this hypothesis and to provide additional insight into the flexibility of NbOFFIVE-1-Ni.

Acknowledgment

H.D. thanks the Scientific and Technological Research Council of Türkiye (TUBITAK) 2214-A Program under the project number 1059B142200109. This research used the computational resources provided for the Quest high-performance computing facility at Northwestern University which is jointly supported by the Office of the Provost, the Office for Research, and Northwestern University Information Technology. This research also used resources of the National Energy Research Scientific Computing Center, a DOE Office of Science User Facility supported by the Office of Science of the U.S. Department of Energy under Contract No. DE-AC02-05CH11231 using NERSC award BES-ERCAP0026844. R.Q.S. acknowledges support from the National Science Foundation under grant no. 2119433. Helpful discussions with Filip Formalik, Xijun Yang, Faramarz Joodaki, and Thang Pham are gratefully acknowledged.

Supporting Information: The versions of NbOFFIVE-1-Ni by changing the order of arrangement of atoms; convergence and error estimation for water adsorption simulations; radial distribution function plot of DFT-optimized structure; comparison of atomic positions of unoptimized and optimized derivatives of NbOFFIVE-1-Ni; effect of electrostatic environment on water uptake of optimized structure; differences in partial atomic charge values for DFT-optimized derivatives at

different water loadings; comparison of simulated water adsorption isotherms for the DFT-optimized derivatives of NbOFFIVE-1-Ni in case of using the same partial atomic charge values; linker rotated derivatives of NbOFFIVE-1-Ni; differences in partial atomic charge values for each atom in the structure of 56.6° rotated linkers; DFT optimization with the initial configurations of unrotated or rotated derivatives in the presence of high gas loading; force field parameters for NbOFFIVE-1-Ni atoms and guest molecules; relative DFT energies, lattice constants and lattice angles of optimized structures, area under the curve (AUC) analysis for CO_2 adsorption isotherms; atomic coordinates and partial charge values of optimized structure; structural properties of derivatives of NbOFFIVE-1-Ni. All derivatives of the MOF are available at https://github.com/hdaglar/Derivatives_of_NbOFFIVE-1-Ni

References

(1) Yaghi, O. M.; O'Keeffe, M.; Ockwig, N. W.; Chae, H. K.; Eddaoudi, M.; Kim, J. Reticular synthesis and the design of new materials. *Nature* **2003**, *423* (6941), 705-714.

(2) Xuan, W.; Zhu, C.; Liu, Y.; Cui, Y. Mesoporous metal–organic framework materials. *Chem. Soc. Rev.* **2012**, *41* (5), 1677-1695.

(3) Farha, O. K.; Eryazici, I.; Jeong, N. C.; Hauser, B. G.; Wilmer, C. E.; Sarjeant, A. A.; Snurr, R. Q.; Nguyen, S. T.; Yazaydın, A. O. z. r.; Hupp, J. T. Metal–organic framework materials with ultrahigh surface areas: is the sky the limit? *J. Am. Chem. Soc.* **2012**, *134* (36), 15016-15021.

(4) Furukawa, H.; Cordova, K. E.; O'Keeffe, M.; Yaghi, O. M. The chemistry and applications of metal-organic frameworks. *Science* **2013**, *341* (6149), 1230444.

(5) Li, H.; Li, L.; Lin, R.-B.; Zhou, W.; Zhang, Z.; Xiang, S.; Chen, B. Porous metal-organic frameworks for gas storage and separation: Status and challenges. *EnergyChem* **2019**, *1* (1), 100006.

(6) Li, D.; Xu, H.-Q.; Jiao, L.; Jiang, H.-L. Metal-organic frameworks for catalysis: State of the art, challenges, and opportunities. *EnergyChem* **2019**, *1* (1), 100005.

(7) Duan, J.; Pan, Y.; Liu, G.; Jin, W. Metal-organic framework adsorbents and membranes for separation applications. *Curr. Opin. Chem. Eng.* **2018**, *20*, 122-131.

(8) Liang, J.; Li, X.; Xi, R.; Shan, G.; Li, P.-Z.; Liu, J.; Zhao, Y.; Zou, R. A robust aluminum metal-organic framework with temperature-induced breathing effect. *ACS Mater. Lett.* **2020**, *2* (3), 220-226.

(9) Schneemann, A.; Bon, V.; Schwedler, I.; Senkovska, I.; Kaskel, S.; Fischer, R. A. Flexible metal–organic frameworks. *Chem. Soc. Rev.* **2014**, *43* (16), 6062-6096.

(10) Qazvini, O. T.; Scott, V.-J.; Bondorf, L.; Ducamp, M.; Hirscher, M.; Coudert, F.-X.; Telfer, S. G. Flexibility of a metal–organic framework enhances gas separation and enables quantum sieving. *Chem. Mater.* **2021**, *33* (22), 8886-8894.

(11) Rogge, S. M.; Goeminne, R.; Demuynck, R.; Gutiérrez-Sevillano, J. J.; Vandenbrande, S.; Vanduyfhuys, L.; Waroquier, M.; Verstraelen, T.; Van Speybroeck, V. Modeling gas adsorption in flexible metal–organic frameworks via hybrid monte carlo/molecular dynamics schemes. *Adv. Theory Simul.* **2019**, *2* (4), 1800177.

(12) Agrawal, A.; Agrawal, M.; Suh, D.; Ma, Y.; Matsuda, R.; Endo, A.; Hsu, W.-L.; Daiguji, H. Molecular simulation study on the flexibility in the interpenetrated metal–organic framework LMOF-201 using reactive force field. *J. Mater. Chem. A* **2020**, *8* (32), 16385-16391.

(13) Devic, T.; Salles, F.; Bourrelly, S.; Moulin, B.; Maurin, G.; Horcajada, P.; Serre, C.; Vimont, A.; Lavalley, J.-C.; Leclerc, H. Effect of the organic functionalization of flexible MOFs on the adsorption of CO 2. *J. Mater. Chem.* **2012**, *22* (20), 10266-10273.

(14) Allen, A. J.; Wong-Ng, W.; Cockayne, E.; Culp, J. T.; Matranga, C. Structural basis of CO_2 adsorption in a flexible metal-organic framework material. *Nanomaterials* **2019**, *9* (3), 354.
(15) Meza-Morales, P. J.; Gómez-Gualdrón, D. A.; Arrieta-Perez, R. R.; Hernández-Maldonado, A. J.; Snurr, R. Q.; Curet-Arana, M. C. CO 2 adsorption-induced structural changes in coordination polymer ligands elucidated via molecular simulations and experiments. *Dalton Trans.* **2016**, *45* (43), 17168-17178.
(16) Amombo Noa, F. M.; Grape, E. S.; Åhlén, M.; Reinholdsson, W. E.; Gob, C. R.; Coudert, F.-X.; Cheung, O.; Inge, A. K.; Ohrstrom, L. Chiral lanthanum metal–organic framework with gated CO2 sorption and concerted framework flexibility. *J. Am. Chem. Soc.* **2022**, *144* (19), 8725-8733.
(17) Kundu, T.; Shah, B. B.; Bolinois, L.; Zhao, D. Functionalization-induced breathing control in metal–organic frameworks for methane storage with high deliverable capacity. *Chem. Mater.* **2019**, *31* (8), 2842-2847.
(18) Mason, J. A.; Oktawiec, J.; Taylor, M. K.; Hudson, M. R.; Rodriguez, J.; Bachman, J. E.; Gonzalez, M. I.; Cervellino, A.; Guagliardi, A.; Brown, C. M. Methane storage in flexible metal–organic frameworks with intrinsic thermal management. *Nature* **2015**, *527* (7578), 357-361.
(19) Forrest, K. A.; Verma, G.; Ye, Y.; Ren, J.; Ma, S.; Pham, T.; Space, B. Methane storage in flexible and dynamical metal–organic frameworks. *Chem. Phys. Rev.* **2022**, *3* (2), 021308.
(20) Formalik, F.; Neimark, A. V.; Rogacka, J.; Firlej, L.; Kuchta, B. Pore opening and breathing transitions in metal-organic frameworks: Coupling adsorption and deformation. *J. Colloid Interface Sci.* **2020**, *578*, 77-88.
(21) Datar, A.; Witman, M.; Lin, L. C. Monte Carlo simulations for water adsorption in porous materials: Best practices and new insights. *AIChE J.* **2021**, *67* (12), e17447.
(22) Zhang, H.; Snurr, R. Q. Computational Study of Water Adsorption in the Hydrophobic Metal–Organic Framework ZIF-8: Adsorption Mechanism and Acceleration of the Simulations. *J. Phys. Chem. C* **2017**, *121* (43), 24000-24010.
(23) Zhai, Y.; Rashmi, R.; Palos, E.; Paesani, F. Many-body interactions and deep neural network potentials for water. *J. Chem. Phys.* **2024**, *160* (14), 144501.
(24) Ho, C.-H.; Paesani, F. Elucidating the competitive adsorption of H2O and CO2 in CALF-20: new insights for enhanced carbon capture metal–organic frameworks. *ACS Appl. Mater. Interfaces.* **2023**, *15* (41), 48287-48295.
(25) Salles, F.; Bourrelly, S.; Jobic, H.; Devic, T.; Guillerm, V.; Llewellyn, P.; Serre, C.; Ferey, G.; Maurin, G. Molecular insight into the adsorption and diffusion of water in the versatile hydrophilic/hydrophobic flexible MIL-53 (Cr) MOF. *J. Phys. Chem. C* **2011**, *115* (21), 10764-10776.
(26) Devautour-Vinot, S.; Maurin, G.; Henn, F.; Serre, C.; Férey, G. Water and ethanol desorption in the flexible metal organic frameworks, MIL-53 (Cr, Fe), investigated by complex impedance spectrocopy and density functional theory calculations. *Phys. Chem. Chem. Phys.* **2010**, *12* (39), 12478-12485.
(27) Coudert, F.-X.; Ortiz, A. U.; Haigis, V.; Bousquet, D.; Fuchs, A. H.; Ballandras, A.; Weber, G.; Bezverkhyy, I.; Geoffroy, N.; Bellat, J.-P. Water adsorption in flexible gallium-based MIL-53 metal–organic framework. *J. Phys. Chem. C* **2014**, *118* (10), 5397-5405.
(28) Grenev, I. V.; Shubin, A. A.; Solovyeva, M. V.; Gordeeva, L. G. The impact of framework flexibility and defects on the water adsorption in CAU-10-H. *Phys. Chem. Chem. Phys.* **2021**, *23* (37), 21329-21337.
(29) Zhou, D.-D.; Zhang, J.-P. On the Role of flexibility for adsorptive separation. *Acc. Chem. Res.* **2022**, *55* (20), 2966-2977.
(30) Daglar, H.; Erucar, I.; Keskin, S. Exploring the performance limits of MOF/polymer MMMs for O2/N2 separation using computational screening. *J. Membr. Sci.* **2021**, *618*, 118555.
(31) Bhatt, P. M.; Belmabkhout, Y.; Cadiau, A.; Adil, K.; Shekhah, O.; Shkurenko, A.; Barbour, L. J.; Eddaoudi, M. A fine-tuned fluorinated MOF addresses the needs for trace CO_2 removal and air capture using physisorption. *J. Am. Chem. Soc.* **2016**, *138* (29), 9301-9307.
(32) Antypov, D.; Shkurenko, A.; Bhatt, P. M.; Belmabkhout, Y.; Adil, K.; Cadiau, A.; Suyetin, M.; Eddaoudi, M.; Rosseinsky, M. J.; Dyer, M. S. Differential guest location by host dynamics enhances propylene/propane separation in a metal-organic framework. *Nature Comm.* **2020**, *11* (1), 6099.

(33) Kresse, G.; Furthmüller, J. Efficient iterative schemes for ab initio total-energy calculations using a plane-wave basis set. *Phys. Rev. B* **1996**, *54* (16), 11169.
(34) Kresse, G.; Joubert, D. From ultrasoft pseudopotentials to the projector augmented-wave method. *Phys. Rev. B* **1999**, *59* (3), 1758.
(35) Blöchl, P. E. Projector augmented-wave method. *Phys. Rev. B* **1994**, *50* (24), 17953.
(36) Grimme, S.; Ehrlich, S.; Goerigk, L. Effect of the damping function in dispersion corrected density functional theory. *J. Comput. Chem.* **2011**, *32* (7), 1456-1465.
(37) Grimme, S.; Antony, J.; Ehrlich, S.; Krieg, H. A consistent and accurate ab initio parametrization of density functional dispersion correction (DFT-D) for the 94 elements H-Pu. *Chem. Phys.* **2010**, *132* (15), 154104.
(38) Perdew, J. P.; Burke, K.; Ernzerhof, M. Generalized gradient approximation made simple. *Phys. Rev. Lett.* **1996**, *77* (18), 3865.
(39) Anisimov, V. I.; Zaanen, J.; Andersen, O. K. Band theory and Mott insulators: Hubbard U instead of Stoner I. *Phys. Rev. B* **1991**, *44* (3), 943.
(40) Tolba, S. A.; Gameel, K. M.; Ali, B. A.; Almossalami, H. A.; Allam, N. K. *The DFT+ U: Approaches, accuracy, and applications*; 2018.
(41) Dubbeldam, D.; Calero, S.; Ellis, D. E.; Snurr, R. Q. RASPA: Molecular simulation software for adsorption and diffusion in flexible nanoporous materials. *Mol. Sim.* **2016**, *42* (2), 81-101.
(42) Rappe, A. K.; Casewit, C. J.; Colwell, K. S.; Goddard, W. A., III; Skiff, W. M. UFF, a full periodic table force field for molecular mechanics and molecular dynamics simulations. *J. Am. Chem. Soc.* **1992**, *114* (25), 10024-10035.
(43) Ewald, P. P. Die Berechnung Optischer und Elektrostatischer Gitterpotentiale. *Annalen der physik* **1921**, *369* (3), 253-287.
(44) Manz, T. A.; Limas, N. G. Introducing DDEC6 atomic population analysis: part 1. Charge partitioning theory and methodology. *RSC Adv.* **2016**, *6* (53), 47771-47801.
(45) Limas, N. G.; Manz, T. A. Introducing DDEC6 atomic population analysis: part 4. Efficient parallel computation of net atomic charges, atomic spin moments, bond orders, and more. *RSC Adv.* **2018**, *8* (5), 2678-2707.
(46) Makrodimitris, K.; Papadopoulos, G. K.; Theodorou, D. N. Prediction of permeation properties of CO_2 and N_2 through silicalite via molecular simulations. *J. Phys. Chem. B* **2001**, *105* (4), 777-788.
(47) Vega, C.; Abascal, J. L. Simulating water with rigid non-polarizable models: a general perspective. *Phys. Chem. Chem. Phys.* **2011**, *13* (44), 19663-19688.
(48) Loos, P.-F. o.; Galland, N.; Jacquemin, D. Theoretical 0–0 energies with chemical accuracy. *J. Phys. Chem. Lett.* **2018**, *9* (16), 4646-4651.
(49) Mardirossian, N.; Head-Gordon, M. Thirty years of density functional theory in computational chemistry: an overview and extensive assessment of 200 density functionals. *Mol. Phys.* **2017**, *115* (19), 2315-2372.
(50) Shukla, P. B.; Johnson, J. K. Impact of loading-dependent intrinsic framework flexibility on adsorption in UiO-66. *J. Phys. Chem. C* **2022**, *126* (41), 17699-17711.
(51) Biovia, D. S. BIOVIA pipeline pilot. *Dassault Systèmes: San Diego, BW, Release* **2017**.
(52) Snurr, R. Q.; Bell, A. T.; Theodorou, D. N. Prediction of adsorption of aromatic hydrocarbons in silicalite from grand canonical Monte Carlo simulations with biased insertions. *J. Phys. Chem. C* **1993**, *97* (51), 13742-13752.
(53) Barsoum, M. L.; Hofmann, J.; Xie, H.; Chen, Z.; Vornholt, S. M.; dos Reis, R.; Burns, N.; Kycia, S.; Chapman, K. W.; Dravid, V. P.; et al. Probing structural transformations and degradation mechanisms by direct observation in SIFSIX-3-Ni for direct air capture. *J. Am. Chem. Soc.* **2024**, *146* (10), 6557-6565.

TOC Graphic:

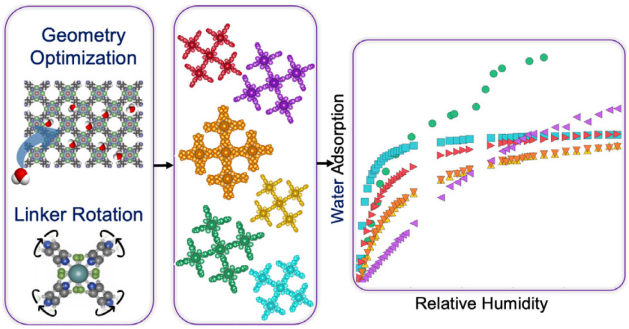
Geometry Optimization
Linker Rotation
Water Adsorption
Relative Humidity